School of Physics

Trinity College Dublin
The University of Dublin

The Fast Transient Sky

Stage Transfer Report

Owen Johnson[†]
Radio Transients Group
March, 2024

Supervisor: Assoc. Prof. Evan Keane

[†]ojohnson@tcd.ie

Abstract

The Universe presents a dynamic canvas of transient objects where rapid changes can be observed over timescales from milliseconds to years. This report details the progress made to answer open questions about an array of objects in the transient sky. This includes the search for exotic subclasses of Pulsars, Fast Radio Bursts, technosignatures, Radio Stars, and Exoplanets.

Contents

Declaration

I hereby declare that this report is entirely my own work and that it has not been submitted as an exercise for a degree at this or any other university.

I have read and I understand the plagiarism provisions in the General Regulations of the University Calendar for the current year, found at http://www.tcd.ie/calendar.

Signed: _____ Date: _____

Publications and Presentations

Publications

Johnson, O.A., Gajjar, V., Keane, E.F., et. al (2023). Simultaneous dual-site SETI with LOFAR international stations. Manuscript accepted for publication to AJ. arXiv:2310.15704

Presentations

1. Low Frequency's Place in SETI, January, 2024, PSETI Symposium, Penn State. [**Invited**]
2. Technosignatures with NenuFAR, December, 2023, Science at Low Frequencies IX, UvA.
   [**Accepted, Presented by Co-Author**]
3. SETI Science at 30 - 190 MHz, November, 2023, BLUK Workshop, SKAO.
   [**Invited**]
4. Technosignature Science at Low Frequencies, November, 2023, NASA Goddard Flight Center.
   [**Invited**]
5. Dual Site SETI Searches, 2023, International Astronautical Congress, Baku.
6. SETI using I-LOFAR, 2023, Irish Astonomy Meeting 23, University College Cork.

Physical Constants

Constant	Symbol	Value
Speed of Light	c	2.99792458×10^{8} m/s
Gravitational Constant	G	6.674×10^{-11} m^3 kg^{-1} s^{-2}
Planck's Constant	h	6.626×10^{-34} m^2 kg s^{-1}
Boltzmann Constant	k_B	1.381×10^{-23} m^2 kg s^{-2} K^{-1}
Stefan-Boltzmann Constant	σ	5.670×10^{-8} W m^{-2} K^{-4}
Electron Charge	e	1.602×10^{-19} C
Electron Mass	m_e	9.109×10^{-31} kg
Proton Mass	m_p	1.672×10^{-27} kg
Neutron Mass	m_n	1.675×10^{-27} kg
Solar Mass	$M_\odot$	1.989×10^{30} kg
Solar Radius	$R_\odot$	6.957×10^{8} m
Solar Luminosity	$L_\odot$	3.828×10^{26} W
Solar Temperature	$T_\odot$	5772 K
Jansky	Jy	10^{-26} W m^{-2} Hz^{-1}

1 A Prelude to Pulsars

When stars with a mass of at least $8\,M_\odot$ reach the end of their evolutionary stage they experience a depletion of nuclear fuel will and undergo a core collapse. This results in the star exploding as a Supernova. Depending on the mass of the host star the Supernova will form a black Hole or a neutron Star. Based on the electron degeneracy pressure limit (Chandrasekhar, 1967, pp. 434 - 443) stars that fall in the range of 20 - 30 $M_\odot$ form neutron stars (Heger et al., 2003).

Neutron stars are supported against further collapse by the presence of neutron degeneracy pressure which arises from the Pauli exclusion principle. Strong Nuclear forces between the neutrons also provides additional support against gravatational collapse. With these two opposing forces a stable equilibrium is formed.

In turn, this makes neutron stars exceptionally dense, they are the densest known objects in the universe that emit light. The average density of a neutron star is 10^{17}kg/m^3 (Baym et al., 1971) and their radii are comparable to the size of cities, with radii of 10 - 20 km.

During collapse the conservation of magnetic flux plays a crucial role in the large strength magnetic fields that are observed in neutron stars along with contributions from the dynamo effect and frozen-in magnetic fields. The strength of a pulsar's magnetic field is on the order of 10^{12} - 10^{15} Gauss (Michel, 1982).

Charged particles accelerate along the magnetic field lines in the magnetosphere of the neutron star. These particles emit electromagnetic radiation in a cone shape along the magnetic axis. If the magnetic axis is not aligned with the rotational axis of the neutron star, the radiation beam will sweep across the sky. This is known as a pulsar, a Galacic lighthouse.

1.1 The Population of Pulsars

At the time of writing there are currently more than 3380 known pulsars. Since their discovery by Jocelyn Bell Burnell (Hewish et al., 1968) the population has grown immensly but there remains many open questions about pulsar evolution and the subclasses that lie within the population as a whole. Similarly to how exoplanet popilations are shown using the mass-radius diagram and stellar populations are shown using the Hertzsprung-Russell diagram, pulsar populations are shown using what is known as the $P-\dot{P}$ diagram.

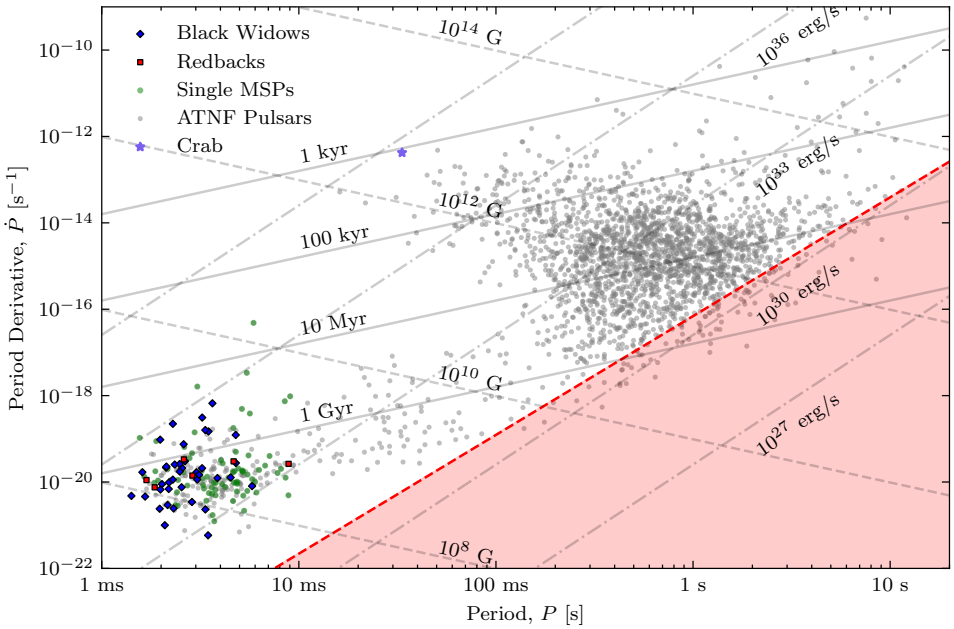

Figure 1.1: The $P-\dot{P}$ diagram showing the population of pulsars. The the milisecond pulsar subclasses are colour coded. The red region represents the death line, where pulsars are theortically no longer able to emit radio waves.

P representing the Pulsar's rotational period and $\dot{P}$ it's derivative. These are key ways that pulsars are classified and study in context of their evolution. An example of a $P-\dot{P}$ diagram is shown in fig. 1.1. Different values on the plot indicate the roughly the Pulsars age and magnetic field strength. Figure 1.1 shows the vastly different values bettween pulsars in the milisecond range and pulsars in the second range.

Theoretically it has been shown that pulsars exhibit a death line in the $P-\dot{P}$ diagram. This is the line where pulsars are no longer able to emit radio waves. This is due to the pulsar's magnetic field is no longer strong enough to accelerate particles along the magnetic field lines. However it has been shown that pulsars do exist below this line. The area below this line is commonly referred to as the "graveyard".

1.2 The Properities of Pulsars

The following section gives a breif non-exhaustive overview of some of the key properities of pulsars.

1.2.1 Neutron Star Radius & Mass

Understanding the mass of pulsars are important for understanding their evolution and equation of state. Oppenheimer and Volkoff (1939) derived a canonical mass limit of neutron stars to be 1.4 $M_\odot$, but expermientally this has been shown to be higher with the largest mass of a pulsar being $\sim 2.35\,M_\odot$ (Romani et al., 2022). The mass-radius relationship of a pulsar is defined by an equation of state and a maximum mass limit. Redshifts and gravatational effects observed in pulsars exhbit the observed temperture and flux to be smaller than the actual value. The observed radius R_{obs} can be described as follows (Lorimer and Kramer, 2004),

$$R_{\text{obs}} = \frac{R}{\sqrt{1-\frac{2GM}{Rc^2}}} = \frac{1}{R}\sqrt{1-\frac{R_s}{R}} \tag{1.1}$$

where R is the pulsar's radius and M is the gravatational mass, G is the gravatational constant, c is the speed of light and R_s is the Schwarzschild radius.
The lower limit of the neutron star radius is decribed by

$$R_{\text{min}} \simeq 1.5\ R_s = \frac{3GM}{c^2} = 6.2\ \text{km}\left(\frac{M}{1.4\,M_\odot}\right) \tag{1.2}$$

Opposite to this the upper limit of the radius is obtained by requiring that there is stability against breaking up due to centrifulgal forces. This gives eq. (1.3) following as described in (Lorimer and Kramer, 2004, p. 58).

$$R_{\text{max}} \simeq \left(\frac{GMP^2}{4\pi^2}\right)^{1/3} = 16.8\ \text{km}\left(\frac{M}{1.4\,M_\odot}\right)^{1/3}\left(\frac{P}{\text{ms}}\right)^{2/3} \tag{1.3}$$

Most pulsars are observed to have radii in the range of 10 - 15 km (Lattimer and Prakash, 2001), giving them the unique position of 'almost' black holes.

1.2.2 Spin Evolution

One of the most unique characterstics of pulsars is the spinning that they exhibit. Understanding the spin evolution gives insight into many parameters of the pulsars most notable the stage of their evolution. Pulsar's begin their life in the upper end of the $P-\dot{P}$ diagram and slowly move down and to the right as they age due to a loss in rotational energy, commonly referred to as spin-down luminosity. The spin-down ($\dot{E}$) is decribed as follows (Lorimer and Kramer, 2004, p. 59),

$$\dot{E} = -\frac{dE_{\text{rot}}}{dt} = 4\pi^2 I \dot{P} P^{-3} \tag{1.4}$$

Where I is the moment of inertia. It is important to note that the energy loss that is converted into radio emmision is almost negligable in comparison to the total energy loss from spin down.

1.2.3 Braking Index

Pulsar's have strong magnetic dipoles, according to classic mechanics a rotating magnetic doplole that exhibts a moment, $|m|$ emits an electromagnetic wave at the pulsars rotation frequency (Lorimer and Kramer, 2004, p. 60). The dipoles radiation power is characterized by,

$$\dot{E}_{\text{dipole}} = \frac{2}{3c^3}|m|^2\omega^4 \sin^2\alpha \tag{1.5}$$

Where α is the angle between the magnetic axis and the rotation axis. Equating the above equation to the loss of rotational energy described in eq. (1.4) gives the following for the expected evolution of the period,

$$\dot{\Omega} = -\frac{2}{3Ic^3}|m|^2\Omega^3 \sin^2\alpha \tag{1.6}$$

This is more commonly written ass a power law,

$$\dot{\nu} = -K\nu^n \tag{1.7}$$

Equation (1.4) in terms of the period is, $\dot{P} = KP^{2-n}$. Since this is a first order differential equation, the solution can be intergrated and given a constant, K which provides and expression of age.

$$T = \frac{P}{(n-1)\dot{P}}\left\{1 - \left(\frac{P_0}{P}\right)^{n-1}\right\} \tag{1.8}$$

Here P_0 is the initial period of the pulsar. Commomly an assumption is made that the current perios is much greater than the intial period ($P_0 \ll P$). If it is also assumped that the pulsar is spinning down to due dipole magnetic radiaiton ($n = 3$), eq. (1.8) can be simplified into a charaactertic age.

$$\tau_c \cong 15.8 \text{ Myr} \left(\frac{P}{s}\right) \left(\frac{\dot{P}}{10^{-15}}\right)^{-1} \tag{1.9}$$

The above estimation for a pulsars age is known to be inconsistent with theorey to varying degrees. In cases where a Supernovae has been observed and produced a pulsar the age is known to a much higher degree of accuracy. The Crab pulsar is one such example with an observed Supernova event in 1054 AD by Chinese astronmers (Kaspi et al., 2001).

1.2.4 Dispersion Measure

The interstellar medium (ISM) is a complex mixture of gas, dust and magnetic fields that fills the space between stars in a galaxy. Given that the ISM is a cold and ionised plasma any electromagnetic radiation will undergo a frequency-depedant index of refraction as they propagate. The following equation describes the refractive index of the ISM neglciting Galactic magnetic field (Lorimer and Kramer, 2004, p. 85),

$$\mu = \sqrt{1 - \left(\frac{f_p}{f}\right)^2} \tag{1.10}$$

Where f_p is the plasma frequency, $8.5 \text{ kHz} \, (n_e/\text{cm}^{-3})^{1/2}$ and f is the frequency of the observed radiation.
If the refractive index of the ISM $\mu < 1$ then it can be assumed that the group velocity of the radiation is $v_g = c\mu$ which is sub light speed. The path of radiotion from a pulsar to the observer will be delayed in time with respect to a infinite frequecy by an amount,

$$t = \left(\int_0^d \frac{dl}{v_g}\right) - \frac{d}{c} \tag{1.11}$$

If is assmumed to be $f_p \ll f$, μ can be approximated.

$$t = \frac{1}{c}\int_0^d \left(1 + \frac{f_p^2}{2f^2}\right) dl - \frac{d}{c} = \frac{e^2}{2\pi m_e c} \frac{\int_0^d n_e \, dl}{f^2} \equiv \mathcal{D} \cdot \frac{\text{DM}}{f^2} \tag{1.12}$$

Where $\mathcal{D}$ is the dispersion constant and DM is the dispersion measure. Each are commonly expressed as follows, $\mathcal{D} = 4.15 \times 10^3 \text{ MHz}^2 \text{ pc}^{-1} \text{ cm}^3 \text{ s}$ and $\text{DM} = \int_0^d n_e \, dl \text{ cm}^{-3} \text{ pc}$. This definition was adapted from Lorimer and Kramer (2004, p. 86) and Taylor and Manchester (1977).

1.3 Pulsar Subclasses

Following breif overview of the properities of pulsars, this section will give a breif overview of the subclasses of pulsars. The population of pulsars can be broken down into subclasses based on unique patterns in their properities. The main subclasses[1] are as follows:

1. Normal Pulsars: These are the most common type of pulsars. They are characterized by their regular pulses and are often observed in radio wavelengths. They are also known as radio pulsars.

2. Rotating Radio Transients (RRATs): These are a subclass of pulsars that were initially discovered through their sporadic radio bursts rather than regular pulses. They exhibit irregular and infrequent radio emission.

3. Magnetars: While not exclusively pulsars, magnetars are highly-magnetized neutron stars that can also emit pulsed radiation. They are characterized by extremely strong magnetic fields, much more intense than typical pulsars.

4. Binary Pulsars: These are pulsars that are in orbit around another star, usually a normal (non-neutron) star. The interaction with the companion star can have significant effects on the pulsar's behavior.

5. Millisecond Pulsars (MSPs): These are pulsars with very short rotation periods, typically less than 10 milliseconds. They are believed to be old pulsars that have been spun up by the accretion of mass from a companion star in a binary system.

6. X-ray Pulsars: Pulsars that emit pulsed X-ray radiation fall into this category. These pulsars are typically observed in binary systems where the pulsar accretes matter from its companion star, leading to X-ray emission.

7. Anomalous X-ray Pulsars (AXPs) and Soft Gamma-ray Repeaters (SGRs): These are closely related to magnetars and are characterized by their intense and variable X-ray and gamma-ray emission. They are believed to be neutron stars with extremely strong magnetic fields.

1.4 Spider Pulsars

The type of pulsar that is of interest to this project is a subclass of transitional millisecond pulsars known as spider pulsars. Spider pulsars fall into two categories depending on their orbiting companion. The first category are known as Black Widow pulsars, segregated based on their companion mass falling in the range of 0.01 - 0.05 solar masses with a

[1] This is a non-exhaustive list.

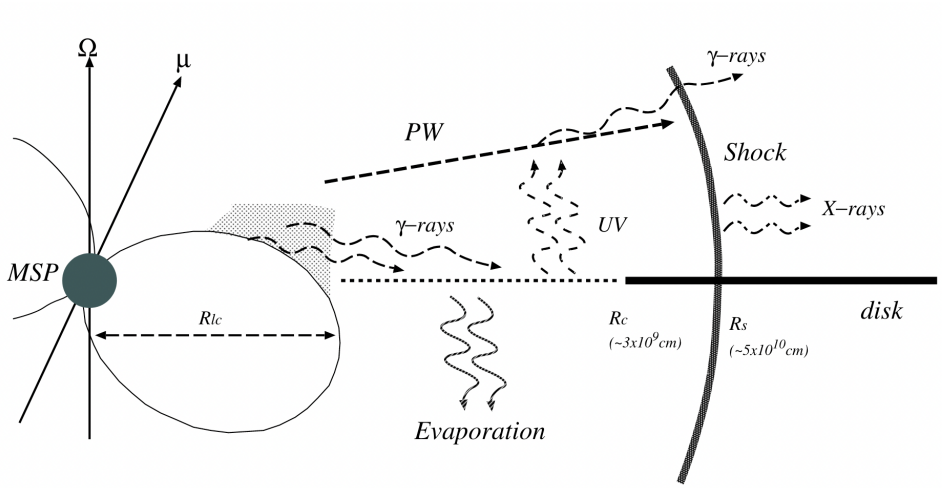

Figure 1.2: Figure taken from Takata et al. (2014). Example of multiwavelength emission from a Redback pulsar.

companion orbital period (P_B) of less than 10 hours (citation). The second category are known as Redback pulsars and have a companion mass of 0.2 solar masses or greater with a P_B of less than 1 day (citation).

It is thought that most millisecond pulsars are formed through the accretion of matter from an evolved compact binary system; the approximately 30% found in isolation are thought to have ablated their companion star to the point of disassociation (citation). Material being thrown off the pulsar causes the radio emission to be eclipsed via scattering and absorption, for a segment of the companion's orbit. Redback systems exhibit both positive and negative period derivatives that are larger than the expected gravitational radiation and are thought to arise from the interaction of the companion's magnetic field and the pulsar's wind (citation).

Redback pulsars have been observed in two transitional states: ablation and accretion states (citation). These states are on sub-year timescales. The transition in stages sees the magnitude of optical emission increase by about one order of magnitude. Studying optical emission from redback pulsars informs on the heating of the companion, Roche-lobe filling fraction, and the mass of the system (citation). Black widow pulsars have been observed to have little to no observable X-ray emission (citation). However, redbacks have been shown to exhibit much more X-ray emission in their thermal spectra with consistent double peaks observable when the pulsar is at inferior conjunction (citation).

The observed companions of redbacks are mostly faint stars with temperatures around X on the farside of the star from the pulsar. The companion's interaction with the pulsar dominates the thermal spectrum of spider pulsars from the present heating between the two. X-ray emission from redbacks shows hard X-ray spectra that follow a power law with photon indices (Γ) around 1 - 1.3. The energy of the thermal spectra in the X-ray is higher than what is expected from shock acceleration. Some models suggest that a wind-

wind shock between the pulsar and companion. However, this approach would require the wind momentum of the pulsar to be much weaker than the companion's. Similarly with the optical emission, the X-ray emission may be influenced by the magnetic field of the companion.

1.5 Why study Redback Pulsars?

Redback pulsars have a number of interesting science cases. Redbacks undergo a range of phenomena, including radio and X-ray pulsations, accretion processes, and periodic eclipses as the companion star passes in front of the pulsar. Their study also provides valuable insights into the evolution of binary systems, the behavior of pulsars, and the physics of accretion processes. Due to their transitional nature, they provide a glimpse into the evolution of pulsars in the latter stages of their life cycle. Pulsars are also used as tools to study theories of gravity, the interstellar medium, and probe for gravitational waves.

1.6 Other exotic transients

Redbacks themselves are exotic transients, but there are many other classes of radio exotic that are of interest to the community. In this project, work has also been carried out on an array of various radio transients and related objects. This includes the search for extraterrestrial intelligence (SETI), the study of M and Brown dwarf radio flares, and the probing of potential radio emission from exoplanets.

1.6.1 Radio Stars and Exoplanets

It has been well documented that our own star, the Sun, and planets in the solar system have radio emission associated with originating from auroras and stellar flares (Murphy et al., 2021; Zarka, 1998). With the advancement of modern radio telescopes, the prospect for capturing radio emission from others and even the prospect of detecting exoplanet magnetospheres has become achievable (Vedantham et al., 2020).

Observing stars especially at low frequency ($\leq$ 300 MHz)[2] act as probes into stellar and planetary plasma environments. Coronal Mass Ejections (CMEs) have a low-frequency burst component in which information about the kinematics of plasma can be deduced (Villadsen and Hallinan, 2019). Incident solar wind is also the primary driving force of auroral emission on magnetized planets. The goal of this project is to explore the viability of detecting radio emission from M and Brown dwarfs using I-LOFAR observations and

[2] $\lambda \sim 1$ m

archive data to put constraints on the prevalence of radio emission from these objects and explore the viability observing radio emission from exoplanets.

Radio emission from stars is typically produced through CMEs, observed phenomenologically in the Sun as type II and III solar bursts. The radio emission from these events is thought to be produced through the electron-cyclotron maser instability (ECMI; Zheleznyakov and Zlotnik, 1975). The ECMI is a plasma instability that occurs in the presence of a magnetic field and a population of energetic electrons. The instability is thought to be the primary driver of radio emission observed in type II bursts and stars as a whole. With type III bursts being thought to be the result of electron beams that are accelerated in the corona.

Emission from planets has also been observed in the form of auroral emission. The most notable example of this is the Jovian system. The Jovian system is known to have auroral emission that is driven by the interaction of the solar wind with the magnetosphere of the planet. Coherent radio emission from the aurora is thought to be produced through the cyclotron maser instability (ECM; Zarka, 1998) which injects a high-velocity electron population into the magnetosphere. The maximum frequency of the ECM is directly proportional to the magnetic field strength of the object at its emitting point (Kavanagh and Vedantham, 2023; Callingham et al., 2024).

Much time has been spent observing Ultracool Dwarfs (M7 <) as they provide a good analogue to the Jovian systems, this allows for direct comparison between the two.

1.6.2 The Search for Extraterrestrial Intelligence

The search for life elsewhere in the universe as always been a burning question for many astronmers throughoout history, even more the previlance of intellgient life in the universe. Since the 1960's there has been consisent surveys, mainly in radio that look for signals of artifical origin, commonly referred to as technosignature. These signatures are thought to be similar to that of radio signals produced artifically on Earth. These signals are mainly thought to be narrowband drifiting radio emission that would be produced by a transmitter leaking into space. To date there has been no positive detection of a technosignature. Similar to dark matter searches, the lack of detections has allowed for limits to be placed on the number of previlance of civilizations in the galaxy. During the first radio SETI survey, Drake (1961) coined an equation to estimate the prevalence of civilizations in the local galaxy.

$$N = R_* \cdot f_p \cdot n_e \cdot f_l \cdot f_i \cdot f_c \cdot L \tag{1.13}$$

Where N is the number of civilizations in the galaxy, R_* is the rate of star formation, f_p is

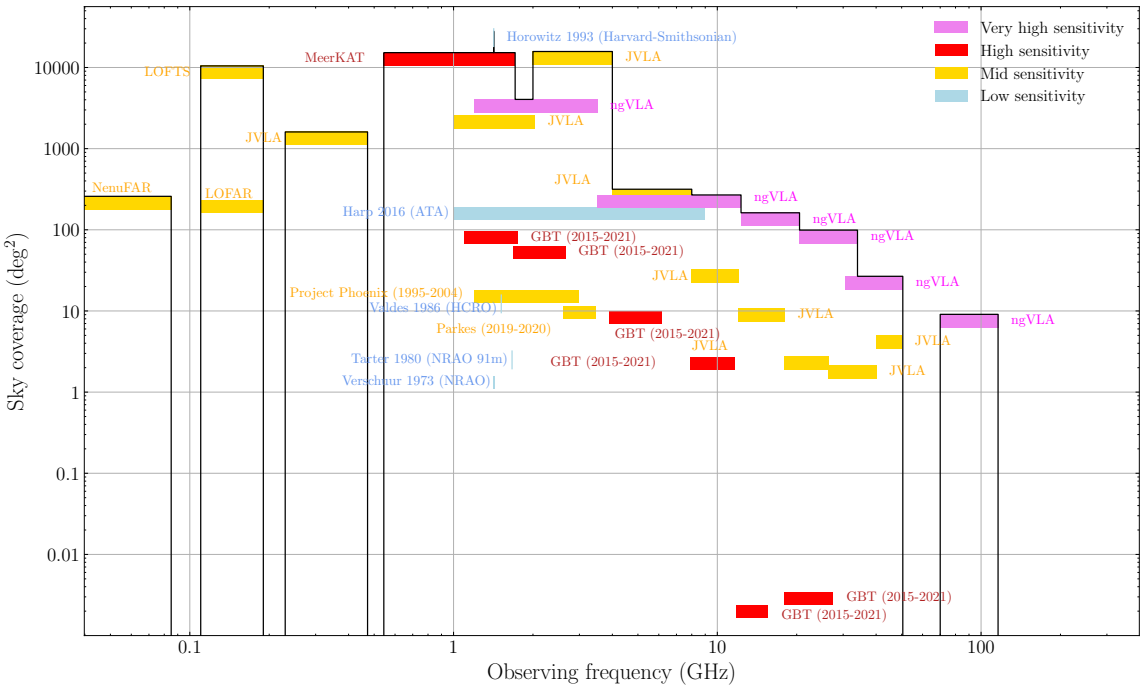

Figure 1.3: The radio frequency parameter space covered by technosignature searches as a function of sky coverage and sensitivity. The color coding represents the ablility to detect an Arecibo-like planetary transmitter at various distances. Where $d_* \leq 25$ pc, $d_* \leq 75$ pc and $d_* \leq 250$ pc are shown in blue, green and red respectively. With anything beyond 250 pc being shown in pink. The figure is adapted from Ng et al. (2022).

the fraction of stars that have planets, n_e is the number of planets that could potentially support life, f_l is the fraction of planets that develop life, f_i is the fraction of planets that develop intelligent life, f_c is the fraction of planets that develop technology, and L is the lifetime of the civilization. However, in this endevour there has been little to no SETI conducted at low frequecies in the radio regime as illustrated in fig. 1.3. The main science goals of a low frequncy technosignature search is to place tight contraints on the Drake equation at these frequencies, study methods on RFI mitgation and also use the high resolution data collected to search and study other radio transients, such as magnetars, Fast Radio Bursts (FRBs), pulsars and M-dwarfs.

2 Pulsar Searching in a Binary System

As outlined in section 1 the study of redback pulsars has a multitude of science cases. However, the number of known redback is small, in searching for new redback pulsars allows for further inquiry into the nature of the subclass. The search usually begins with the selection of potential candidates from large-scale surveys carried out by optical, X-ray and γ-ray observatories. Candiates are determined based on the flaring exhibted at these shorter wavelengths, then followed up using radio telescopes. Work to date has been to perform follow-up radio observations of Redback candidates to attempt to confirm radio emission and further compliment prior multiwavelength studies.

The *Fermi* Large Area Telescope (LAT) provides the most candidates as the related γ-ray emission are not subject to the same limitations as other detection methods (Ray et al., 2012). Both candidates observed so far as part of this project are two Fermi candidates 1FGL J0523.5-2529 and 4FGL J2054.2+6904.

2.1 Observation Campaigns

J0523 was the first observed candidate and was observed using the Ultra-Wide-Bandwidth, Low Frequency Reciver (UWL)[3] on the Parkes Murriyang telescope in New South Wales. Published studies from Strader et al. (2014) and Halpern et al. (2022) provide the orbital period, companion's radial velocity and distance measurements for the system. Each of these factors are important in determining the observation and search strategy.

For the pulsar to be detected the radio emission from the poles must be visible to the observer plane of view and the beam must be unobsured by the companion star. The orbital phase can be easily calculated from the periodic emission in the optical as demonstrated in fig. 2.1 using the following equation,

$$\phi = \frac{t - T_0}{P_{\text{orb}}} \tag{2.1}$$

At the time of writing 74% of the orbital phase has been observed, with time approved to observe the remaining orbital phase if the pulsar is not detected.

In the case of J2054 less information is known with no accurate phase ephermeris avalible. A study by Karpova et al. (2023) reports the period, companion radius and distance. Over 8 hours of observations have been carried out using I-LOFAR. In this case the entire orbit

[3]The UWL operates from 704 to 4032 MHz (40 - 7 cm)

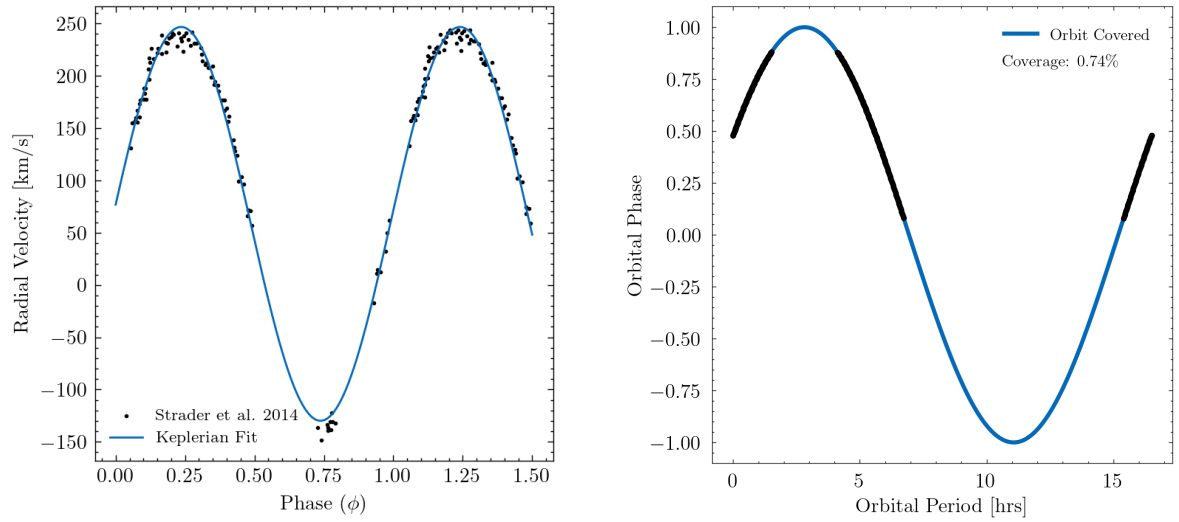

(a) **(b)**

Figure 2.1: *(a)* Phased radial velocities observed from the optical counterpart of J0523 with the Keplerian fit overplotted. *(b)* Observed oribital phase of J0523 with Parkes UWL to date.

needs to be covered and blindly searched for radio emission within expected parameter range of a Redback pulsar. Observations with X are planned to take place in the Summer of 2024 to try and determine the orbital phase based.

2.2 Observation Data

Observations from radio telescopes typically includes measurements of intensity, frequency, polarization and time. The data is usually stored in a time series format with the intensity and frequency measurements recorded at each time step. The data is usually stored in a filterbanks (`.fil`) or .fits file format. The raw voltages are recorded and then processed into usable Stoke I files.

2.3 Search Strategy

A zoo of pulsar software has been developed over the past decades to detect and time pulsars. One of the most commonly used softwares in the search for binary pulsars is PRESTO (Ransom, 2001). The search is carried out as illustrated in fig. 2.2 and due to the large data volumes produced by modern telescopes, the search is carried out in a distributed manner on high performance computing clusters.

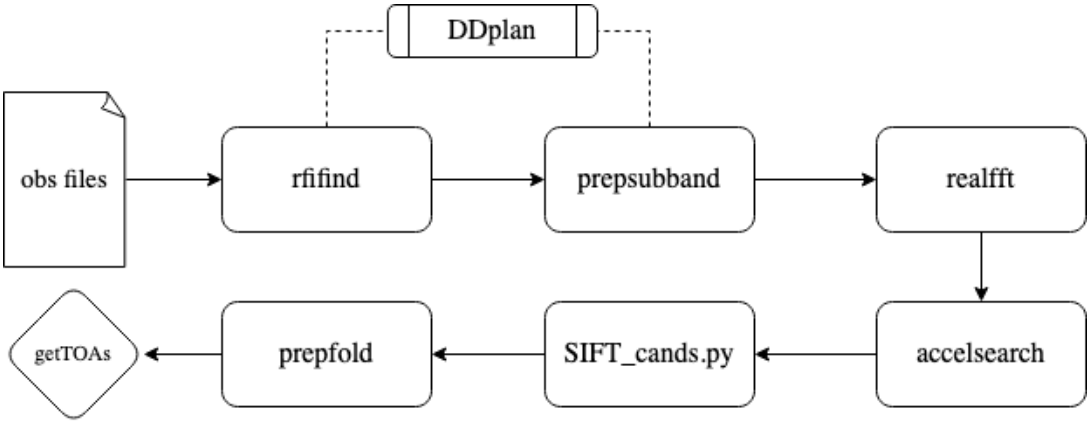

Figure 2.2: Outline of the PRESTO search strategy used to search for binary pulsars.

2.3.1 RFI Removal

The first step in nearly all radio observations is to remove Radio Frequency Interference (RFI) from the observations data, this is usually caused by most modern technologies. This is important as artifical signals can mimic period signals associated with pulsar emission. Thus the data must mask frequencies or be clipped in the time domain. This project makes use of `rfifind` to remove such RFI.

`rfifind` which is part of the PRESTO suite searches in both frequency and time domains. It analyses each channel for a specified time integration. Firstly the time domain statitics are computed which consists of the mean and stadared deviation of the values in each channel. For blocks where the mean value exceeds 4σ the block is flagged as RFI. If more than 30% of the channel is flagged the entire channel is masked completely and replaced with a median constant bandpass value. An example of a mask produced by `rfifind` is shown in fig. 2.4.

2.3.2 Incoherent Dedispersion

Following the masking of all observation files the next step is to inchoherently dedisperse the data. This is done to remove the effects of dispersion caused by the interstellar medium as discussed in X. Failure to de-disperse data broadens potential pulse profiles and significantly reduces the signal to noise ratio. Figure 2.3 shows an example of pulse dispersion. Inchoherent dedispersion is carried out by splitting the data into subbands and then shifting the data in time to correct for the desipersion.

When correcting for dispersion it is important to consider the possible range of DMs that the pulsar could exhibit. The DM can be estimated through the use of density electron models such as X and X. However when dedisperseing the data it inherently induces smearing in the data. There are four types of smearing that need to be acounted for and characterized by the following equation,

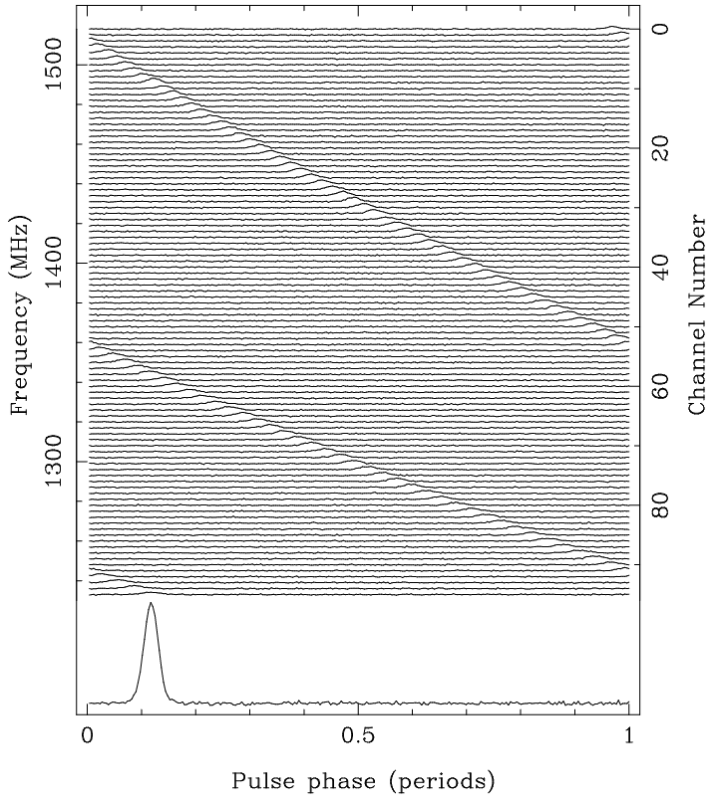

Figure 2.3: Example of a dispersion pulses of 128 ms pulsar B1356-60, which has a dispersion measure of 295 pc cm^{-3}. Figure from Lorimer and Kramer (2004, p. 20).

$$\tau_{\text{total}} = \sqrt{\tau_{\text{samp}}^2 + \tau_{\text{sub}}^2 + \tau_{\text{BW}}^2 + \tau_{\text{chan}}^2} \tag{2.2}$$

2.3.3 Fast Fourier Transform

The data is needs to be transformed into the frequency domain to search for periodic signals. This is commonly done with a Discrete Fourier Transform (DFT) in pulsar astronomy and computationally carried out using a Fast Fourier Transform (FFT). For a time series, S_j of a given length of N it is neccessary to convert the time series into the barycentric frame of reference. The barycentric frame if reference point is centered on the mass of the solar system.

The kth Fourier component of the time series is described in Lorimer and Kramer (2004, pp. 132-134) as,

$$\mathcal{F}_k = \sum_{j=0}^{N-1} S_j \exp\left(-2\pi\sqrt{-1}\frac{jk}{N}\right) \tag{2.3}$$

To complete this computation it requires N^2 floating point opearations. However, if a FFT operation is employed the number of operations is reduced to $N \log_2 N$ for a time

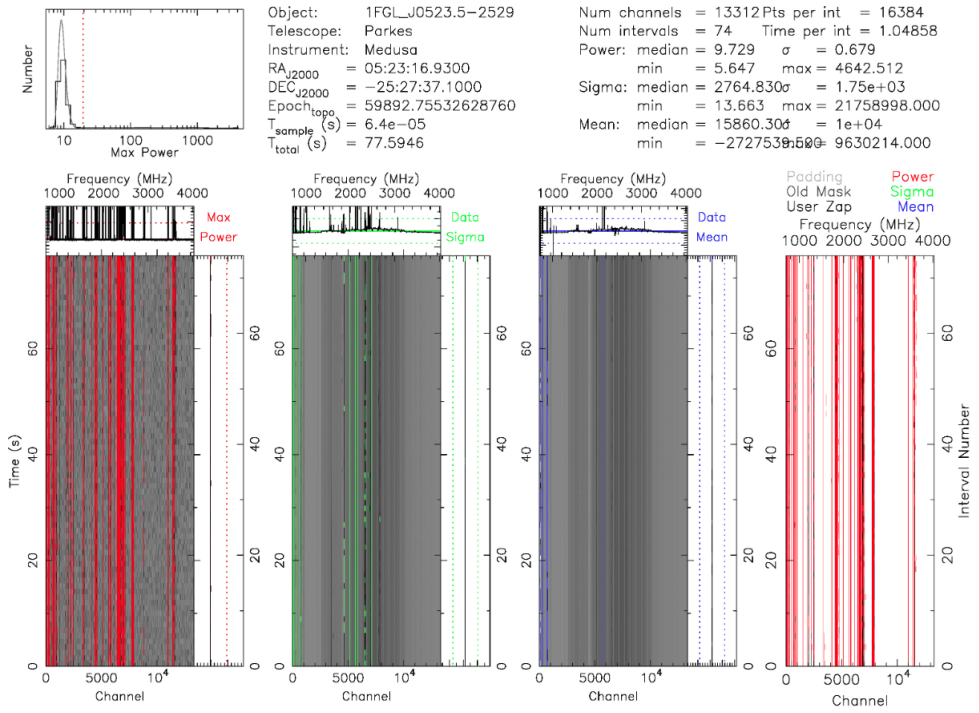

Figure 2.4: Example of RFI removal using `rfifind` on a 77 second observation of J0523. The upper left panels shows the max power profile of the RFI detected. The bottom most left panel show the max power, the second panel to the right shows the σ, the third panel shows the mean and the right most panel is the reccomended mask with all panels plotted.

series of length N. Since the time series data are real numbers symmetry can be exploited as the DFT is symmetric about the Nyquist frequency, $\nu_{\text{Nyq}} = 1/(2t_{\text{samp}})$. For any frequencies higher than the ν_{Nyq} the complex conjucate is the same as the corresponding lower half of the frequency.

On the software side this is carried out with the `realfft` function in PRESTO. This result intakes the dedisperesed subbands and returns the power spectrum of the data. At this point the data is in a state to be searched for periodic signals.

2.3.4 Accelration Searching

Searching for binary pulsars requires a slightly different approach as the motion of the system causes the observed pulse frequency to smear across the Fourier bins (Cherry's paper), in turn this reduces the sensitivity of the search. A solution to this is to split up the search into smaller time intervals and assume that the radial velocity is a constant on this time scale. This can be shown to be a good approximation for $P_b/10$.
The spin frequency, f_{spin} and the time of pulse emission, t_{pulse} the pulsar's phase can be expressed as, $\phi_p = f_{\text{spin}} t_{\text{pulse}}$. Morever, the pulse time can be expressed as the time of arrival from the pulsar, $d(t_0)$,

$$t_{\text{pulse}} = t_0 - \frac{d(t_0)}{c} \tag{2.4}$$

thus the phase can be expressed as,

$$\phi_p = f_{\text{spin}} \left[t_0 - \frac{d(t_0)}{c} \right] \tag{2.5}$$

$$= f_{\text{spin}} \left[t_0 - \frac{a \sin i}{c} \sin \left[\frac{2\pi(t - t_{\text{asc}})}{P_B} \right] \right] \tag{2.6}$$

where a is the semi-major axis, i is the inclination angle, t_{asc} is the time of ascending node and P_B is the orbital period. A Taylor expansion can be used to $\sin x$ around $x = a$ such that,

$$\sin(x) \simeq \sin(a) + \cos(a)(x - a) - \frac{\sin(a)}{2!}(x - a)^2 - \frac{\cos(a)}{3!}(x - a)^3 + \dots \tag{2.7}$$

Therefore the phase of the pulsar with a constant spin down rate can be expressed as,

$$\phi(t) = f^1 t_0 + \frac{\dot{f}}{2}(t - t_0)^2 + \frac{\ddot{f}}{6}(t - t_0)^3 + \dots \tag{2.8}$$

Matching co-effcients between the the full Taylor expansion and the phase expression for the pulsar gives the following relation, $\dot{f}/2 = f_{\text{spin}} \frac{a \sin i}{c} A$. Where A is represents all the terms in the expansion. The final simplified expression works out to be,

$$\dot{f} = f_{\text{spin}} \frac{4\pi^2 a \sin i}{c P_B^2} \sin \left[\frac{2\pi(t - t_{\text{asc}})}{P_B} \right] \tag{2.9}$$

Thus over a small enough time period spin-down is approximately constant.

$$\frac{k_2 P_B}{2\pi q} = a \sin i \tag{2.10}$$

Where k_2 is the radial velovity semi-amplitude, P_B is the orbital period and q is the mass ratio.

Searching is carried out using `accelsearch` which searches the FFT time series for period emissions by summing the highest Fourier frequency derivative. The number of bins that this signal is smeared is given by the acceleration parameter (Ransom, 2001),

$$z \simeq \dot{f} T_{\text{obs}}^2 \tag{2.11}$$

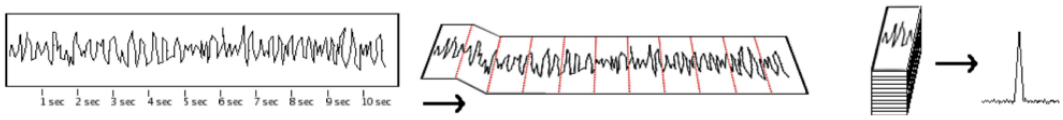

Figure 2.5: Adapted illustration from X of the folding process. The left panel shows the observed time series, the middle panel shows the folded time series and the right panel shows the summed pulse profile.

Where T_{obs} is the length of the observation. The search is carried out over a range of accelerations which can be based on eq. (2.10) if the physical quantities are known. A list of the known orbital parameters for the two candidates is given in table 1 along with resultant z values.

Candidate	P_{orb} (days)	k_2 (kms^{-1})	$a \sin i$ (s)	e	q	z
J0523.5-2529	0.68813	190.3	0.359	0.040	0.61 ± 0.06	
J2054						

Table 1: Orbital parameters of the two candidates. Values for J0523 are taken from Strader et al. (2014) and Halpern et al. (2022). Values for J2054 are taken from Karpova et al. (2023).

In cases where the orbital parameters are not known the search is carried out over a range of accelerations from 0 to 200, and even in the case where the value exceeds 200, this is left as a cap on the search. The reason that the search is not carried out over the entire range is due to the computaitonal cost and is often not neccessary with accelerations above 200 starting to exhibit a non-linear relationship as stated in Ransom (2001). Once the search is carried out the results are outputted in the form of candidates with estimates on DM, S/N, period and frequecies.

2.3.5 Folding and Timing

Pulsar folding is a technique commonly used when the pulses are not bright enough to be clearly visible in the observed time series. The term folding comes from the fact that the time series is folded on itself by some trial period of the pulsar, this is illustrated in fig. 2.5.

Using a routine called `prepfold` each of the candiates over the noise floor are folded with each candidate examined by eye for possible postive pulsar detection. An example of this is shown in fig. 2.6. This plot contains integrated pulse profile, time series plot and subband plot. It also shows DM, P and $\dot{P}$ plots as a function of reduced χ^2 values.

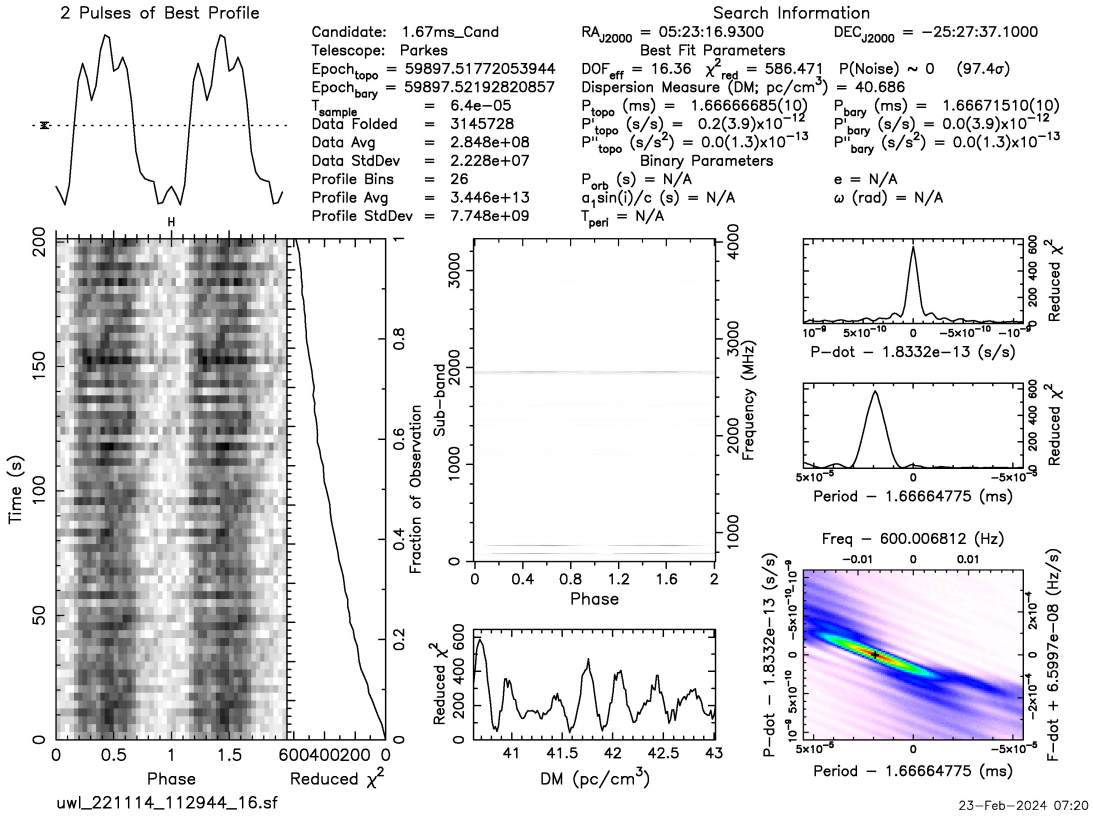

Figure 2.6: Example of a `prepfold` plot for a candidate.

3 Technosignature Searches at Low Frequencies

The first year of the project primarly entailed the publication (Johnson et al., 2023) of results from the first search for technosignatues at low frequency using Irish and Swedish LOw Frequency ARay (I-LOFAR; van Haarlem et al., 2013). When carrying out this technosignature search the two main goals were to constrain the prevalance of intellgient civilizations in the Milky Way at an unexplored frequency and use the collected data to search for other exotic transients such as Fast Radio Bursts (FRBs), pulsars, magnetospheres and M-dwarf emission (Sheikh, 2020). The following sections will detail the means and methods on how technosignature search is carried out.

3.1 LOFAR

LOFAR, a pioneering low-frequency aperture array telescope, spans hundreds of kilometers across Europe and serves as a pathfinder to the Square Kilometer Array (SKA). The array consists of a core station with outrigger stations situated in the Netherlands and additional international stations spanning multiple countries, such as Germany, France, Sweden, Ireland, Latvia, Poland, and the United Kingdom. Additionally, stations are currently in the process of being constructed in Italy and Bulgaria. The LOFAR array operates using two types of antenna, the Low Band Antenna (LBA) and the High Band

Antenna (HBA), operating at 10–90 MHz and 100–250 MHz respectively. In this study, the HBAs at the Irish and Swedish LOFAR station are used to carry out observations noninterferometrically. The field of view (FoV) of an international LOFAR station is rather large; at full width at half maximum, it is 5.3, 3.4, and 2.3 deg^2 at frequencies of 120, 150, and 180 MHz, respectively (van Haarlem et al., 2013). The station is capable of resolution of 3.3 and 0.2 arcsecond at the bottom and the top of the bad respectively when the entire array is in use making it one of the most sensitive telescopes in the world.

3.2 Target Selection

A significant fraction of radio emission from Earth is emitted in the direction of the ecliptic plane. For example, powerful planetary radars are used to explore Solar System objects (Siemion et al., 2013), and high-powered transmitters are used to communicate with Solar System probes (Enriquez et al., 2017). It is conceivable then that such leakage radiation may also be emanating from other worlds, preferentially in their planetary orbital planes. This is why we chose TESS targets, as these are the closest transiting exoplanet systems known (Borucki et al., 2010; Ricker et al., 2015). Observing these sources with the LOFAR HBAs enables robust constraints on any associated artificial low-frequency radio emission

3.3 Expanding the Cosmic Haystack

Searching for technosignatures is akin to searching for a needle is a cosmic sized haystack thus it is important to extend area of the haystack as much as possible. The beam of a LOFAR station has an expansive coverage enabling observation of a substantial number of stars in the field of view. The significance of these in-field stars has been highlighted by Wlodarczyk-Sroka et al. (2020). Consequently, during our observations targeting 44 sources from the TESS catalog, we encountered a significant number of in-field stars within our field of view, as shown in **add Figure 2**. To determine the list of targets within this field of view, the Gaia catalog is utlizied. Some previous major SETI surveys focused their searches toward Sun-like stars (Tarter, 1996). However, because our understanding of the origin of life is limited, it makes sense to allow for the possibility of life arising on a planet that is neither Earth-like nor around stars that are Sun-like. Similarly, planets not necessarily located in the habitable zone should be considered. This is typically characterized as the orbital range wherein liquid water could exist (Kasting et al., 1993), as inferred from planetary equilibrium temperatures often ignoring the unknown albedo of the exoplanets. Any sensitive radio SETI survey seeking to maximize the chance of detecting weak radio signals should, insofar as possible, expand its search to encompass nearby stars of a broad range of spectral types and with exoplanets of all sizes

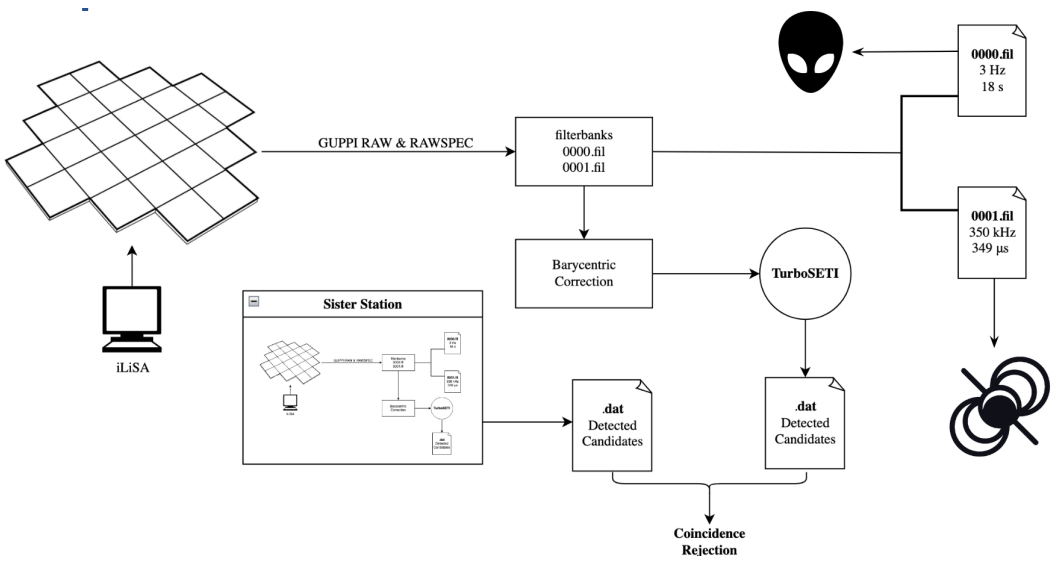

Figure 3.1: Outline of the SETI pipeline developed and deployed on Breakthrough Listen nodes at both LOFAR stations.

and distances from their parent star. Thus, calculations were conducted to determine the number of Gaia stars with a mean distance of 1215 pc, with an accuracy in their distances of at least 20%. This study used Gaia's third data release (GDR3; Gaia Collaboration et al., 2023; Ginsburg et al., 2019). When analyzing GDR3, two filters were applied to the survey volume and sensitivity accuracy of the in-beam target values. First, a constraint on the R.A. and decl. errors was implemented. If a Gaia source was found to be in the beam but had an error magnitude greater than the FWHM, it was removed from the source pool. Equation (3.1) states the first condition of filtering:

$$\theta_{\text{sep}} + \sqrt{\Delta\text{RA}^2 + \Delta\text{Dec}^2} \leq \frac{\text{FWHM}}{2} \tag{3.1}$$

As the sensitivity of the survey is calculated based on a source's distance, a second filter is implemented to remove sources that have large errors. By taking the difference ($\Delta\sigma_G$) in the upper and lower confidence levels of GSP-Photometry, we obtain a percentage error on distance. All sources with a d_{M_G} error of 20% or greater are filtered out of the source list. Equation (3.2) states the second condition of filtering:

$$\frac{\Delta\sigma_G}{\sigma_G} \leq 20\% \tag{3.2}$$

A total of 1,631,152 stars form this list, making it one of the largest samples of stars ever surveyed for SETI purposes.

3.4 Carrying out a Dual-Site Survey

Typically, international LOFAR stations operate as standalone telescopes $2-3$ days per week, i.e. they do not operate as part of the International LOFAR Telescope's Europe-wide array. This project was undertaken during this standalone time. For this purpose the *international LOFAR in Stand-Alone mode* (`iLiSA`) package[4] is used to control both telescopes simultaneously. `iLiSA` provides a high-level operational control of multiple LOFAR stations, including scheduling, processing pipeline dispatching and metadata aggregation. For the observations in this study, an operator-produced list of targets that were close[5] to the local meridian was fed into `iLiSA` at each epoch. Towards each target, one beam per station was formed using `iLiSA`, and each beam was formed with 412 HBA sub-bands (corresponding to a bandwidth of 80.46875 MHz). The scan time on each target was 15 min, and the whole scheduling block was a few hours per epoch. Data was preproccessed[6] and prepared using the `udpPacketManager` package (McKenna et al., 2023). Which resulted in two sets of filterbanks for each observation, each with different frequency and time resolutions. The first set of filterbanks had a frequency resolution of 2.98 Hz and a temporal resolution of 0.67 s. The second set of filterbanks had a frequency resolution of 350 kHz and a temporal resolution of 349 μs. The first set of filterbanks was used for the search for narrowband technosignatures, and the second set was used for the search for broadband transients. A broad overview of the pipeline employed is shown in fig. 3.1.

3.5 Narrowband Search Results

Using *turboSETI*, a Doppler-drift search was carried out on the observed candidates at both stations. This resulted in the list of "hits" collected, where hits are defined as a narrowband signal detected above the given threshold, S/N = 10. The distribution of narrowband signals detected at both stations is shown in Fig X. A large percentage of hits are seen at both sites in the 120-140 MHz range. This falls within the range of expected RFI leakage seen from neighboring airports[7]. Using a drift-rate search of ± 4 Hz/s for this study covers a fraction of the possible drift rates of transmitters from exotic objects that can be detected as outlined by Sheikh et al. (2019). Li et al. (2022) shows that 4 Hs/s is comprehensive in relative to the expected distribution of exoplanet drift rates. The omission of a search in this parameter space is due to its computationally intense nature of searching for narrow-band signals across a sizeable drift-rate range. However, in doing

[4] https://github.com/2baOrNot2ba/iLiSA/releases/tag/v6.1

[5] In practice as Birr and Onsala are separated by ~ 20 deg of longitude, the optimum scheduling is to observe ~ 40 min$-T_{\rm obs}/2$ 'late' at Onsala and 40 min$+T_{\rm obs}/2$ 'early' at Birr.

[6] For detailed explanation of the preprocessing and preperation see Lebofsky et al. (2019)

[7] Shannon & Goteborg Landvetter.

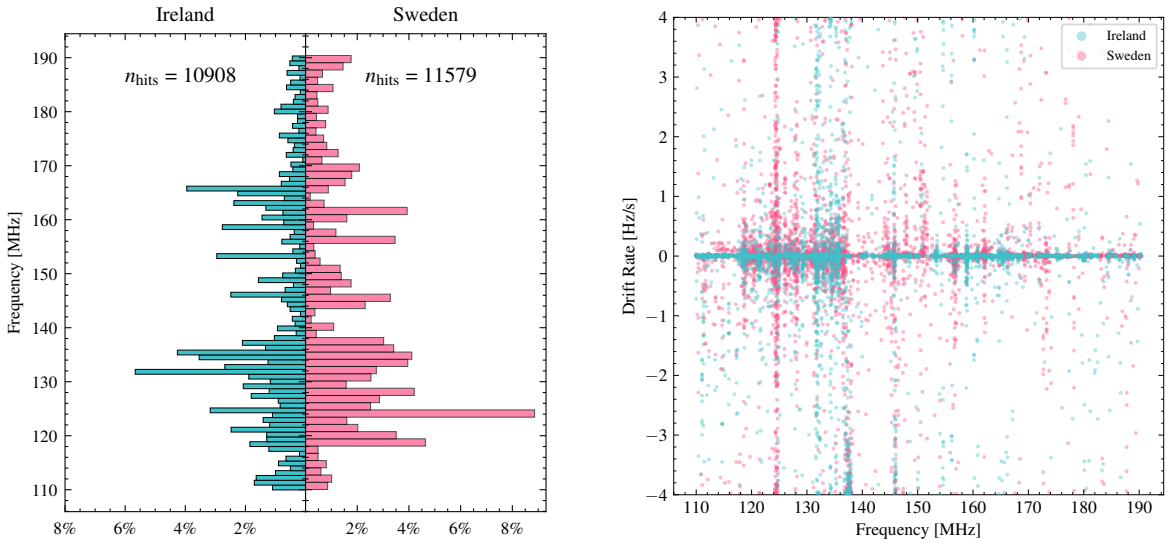

Figure 3.2: *(a)* Comparison of drifting signals or "hits" detected at both stations seen across the HBA frequency band. Each bin within the data set represents a 1 MHz frequency range and is accompanied by a corresponding percentage indicating its proportion to the overall data set. *(b)* A scatter plot of the drift-rate values against detected frequency. The Irish station is shown in pink and the Swedish station is shown in blue.

this, the parameter space searched for ETI signal has been drastically reduced. Continual development of search algorithms like `turboSETI` is progressing to make larger drift-rates searches a more computationally feasible. Upon first inspection of Figure 3.2 it appears that the results at both stations are somewhat similar. However, upon performing a Kolmogorov-Smirnov (KS) test for each set of results for drift-rate, SN and frequency of detected hits the highest p-value returned was on the order of 10^{-11} indicating that the RFI environments at each of the stations are significantly different. In the case of this study, a singular beam observes a single target for 15 minutes at both stations and observations are converted to barycentric reference frame. Narrow-band searches are then performed at both sites, and the results of both searches are compared.

In our analysis, a signal is classified as a mutual extraterrestrial hit only if two conditions are met: *a)* the signals are within a frequency range of ±4 Hz of each other in the barycentric reference frame, and *b)* their drift rates are within ±0.2 Hz/s of each other after barycentric drift corrections. In Figure **??**, an intriguing candidate is depicted. In the topocentric frame, we detected a narrowband signal at 160 MHz that was simultaneously present at both stations. However, when converting to the barycentric reference frame (as illustrated in Figure **??**), the signal appears to be seen at different frequencies with opposite signs due to the different line-of-sight velocities towards the target. As a result, this narrowband signal is rejected as a genuine sky-bound signal.

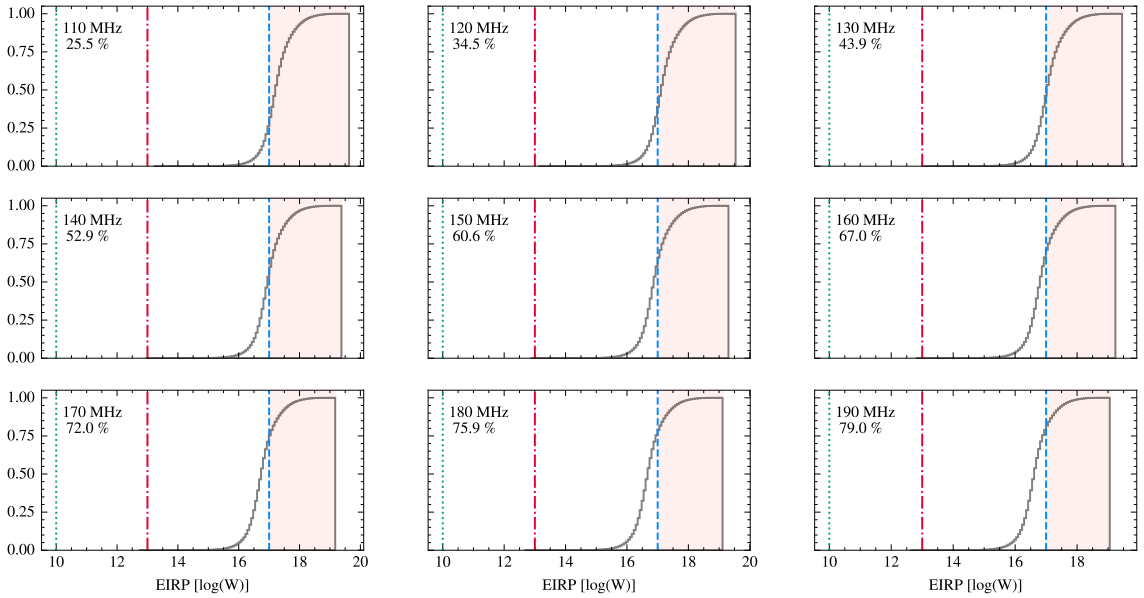

Figure 3.3: Cumulative histogram of EIRP limits of this survey across the HBA band. Reference luminosities for three civilization Kardeshev levels emitting 10^{17},10^{13} or 10^{10} W are shown in blue, red, and green respectively. The percentage of targets where the station is sensitive to the transmission of 10^{17} W is shown, as a function of frequency across the band. At lower frequencies, sensitivity to 10^{17} emitters drops off as the $T_{\rm sys}$ rises. The $\bar{T}_{\rm sys}$ varies from 1260 K down to 322 K as frequency is increased across the band. Detailed calculations are presented in Appendix B of Johnson et al. (2023).

3.6 Constraints placed by the Survey

4 Forward Plan

As of writing this there has been a single publication from this project (outlined in section 3) with numerous other in preparation. Figure 4.1 outlines the estimated timeline for the completion of all outlined projects.

NenuSETI has had 80% of the analysis complete. This paper is currently being drafted and once some system adminstration with the BL backend in Nancay is complete, the paper will be swiftly submitted no latter than the end of April 2024.

Redback Pulsar Search has full analysis pipelines written and deployed on the OzStar supercomputing cluster in Swinburne and REALTA backend in Birr. As of writing, all data from J2059 has been processed with expanded trials commencing to try and find the pulsar. Processing on J2054 is 50% complete but temporarily halted due to some bottlenecking on the backend. Expected publication date of either a pulsar detection or non-detection is expected by the end August 2024.

LOFTS as previously discussed in X, the observation campaign is expected to commence following the roll out of LOFAR 2.0 upgrades to the core stations in the Netherlands.

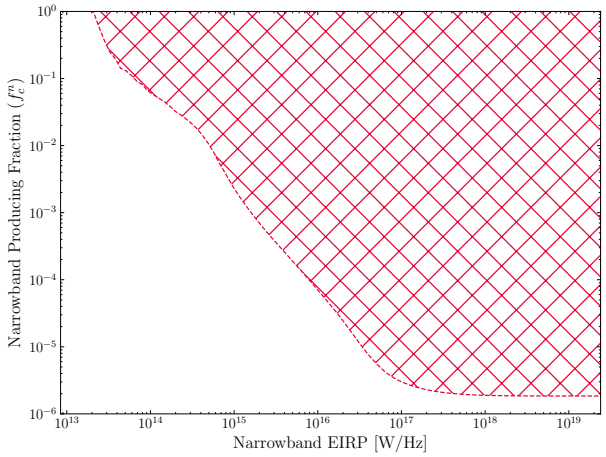

Figure 3.4: The fraction of stars that produce narrow-band emission (f_c^n) against the transmitter power of the total target pool. The hashed region (red) shows the constraints this survey places on a value of f_c^n at 110 - 190 MHz.

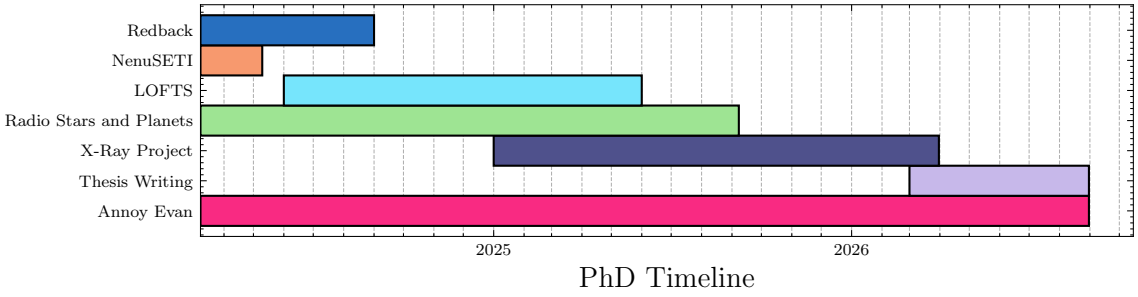

Figure 4.1: Estimated timeline for compleltion of these projects which was covered in . Each increment on the grid is equivalent to 1 month.

This is expected to happen in the early Summer months of 2024. This will cause all remote stations to be given 100% of observing time, thus the large amount of observation time for LOFTS can be accomidated.
Automated pipelines to handle the data are written and tested on operational backends. Deployment of BL backend to the Chilboltan station is expected to be completed in the coming months.

Radio Stars and Planets

X-ray Project

5 Conclusion

References

Baym, G., Bethe, H. A., and Pethick, C. J. (1971). Neutron star matter. *Nuclear Physics A*, 175(2):225–271.

Borucki, W. J., Koch, D., Basri, G., Batalha, N., Brown, T., Caldwell, D., Caldwell, J., Christensen-Dalsgaard, J., Cochran, W. D., DeVore, E., Dunham, E. W., Dupree, A. K., Gautier, T. N., Geary, J. C., Gilliland, R., Gould, A., Howell, S. B., Jenkins, J. M., Kondo, Y., Latham, D. W., Marcy, G. W., Meibom, S., Kjeldsen, H., Lissauer, J. J., Monet, D. G., Morrison, D., Sasselov, D., Tarter, J., Boss, A., Brownlee, D., Owen, T., Buzasi, D., Charbonneau, D., Doyle, L., Fortney, J., Ford, E. B., Holman, M. J., Seager, S., Steffen, J. H., Welsh, W. F., Rowe, J., Anderson, H., Buchhave, L., Ciardi, D., Walkowicz, L., Sherry, W., Horch, E., Isaacson, H., Everett, M. E., Fischer, D., Torres, G., Johnson, J. A., Endl, M., MacQueen, P., Bryson, S. T., Dotson, J., Haas, M., Kolodziejczak, J., Van Cleve, J., Chandrasekaran, H., Twicken, J. D., Quintana, E. V., Clarke, B. D., Allen, C., Li, J., Wu, H., Tenenbaum, P., Verner, E., Bruhweiler, F., Barnes, J., and Prsa, A. (2010). Kepler Planet-Detection Mission: Introduction and First Results. *Science*, 327(5):977–.

Callingham, J. R., Pope, B. J. S., Kavanagh, R. D., Bellotti, S., Daley-Yates, S., Damasso, M., Grießmeier, J.-M., Güdel, M., Günther, M., Kao, M. M., Klein, B., Mahadevan, S., Morin, J., Nichols, J. D., Osten, R. A., Pérez-Torres, M., Pineda, J. S., Rigney, J., Saur, J., Stefánsson, G., Turner, J., Vedantham, H., Vidotto, A. A., Villadsen, J., and Zarka, P. (2024). Radio stars and exoplanets. *Nature Astronomy*.

Chandrasekhar, S. (1967). *An Introduction to the Study of Stellar Structure*. Dover Books on Astronomy Series. Dover Publications, Incorporated.

Drake, F. D. (1961). Project Ozma. *Physics Today*, 14(4):40.

Enriquez, J. E., Siemion, A., Foster, G., Gajjar, V., Hellbourg, G., Hickish, J., Isaacson, H., Price, D. C., Croft, S., DeBoer, D., Lebofsky, M., MacMahon, D. H. E., and Werthimer, D. (2017). The Breakthrough Listen Search for Intelligent Life: 1.1-1.9 GHz Observations of 692 Nearby Stars. *The Astrophysical Journal*, 849:104.

Gaia Collaboration, Vallenari, A., Brown, A. G. A., Prusti, T., de Bruijne, J. H. J., Arenou, F., Babusiaux, C., Biermann, M., Creevey, O. L., Ducourant, C., Evans, D. W., Eyer, L., Guerra, R., Hutton, A., Jordi, C., Klioner, S. A., Lammers, U. L., Lindegren, L., Luri, X., Mignard, F., Panem, C., Pourbaix, D., Randich, S., Sartoretti, P., Soubiran, C., Tanga, P., Walton, N. A., Bailer-Jones, C. A. L., Bastian, U., Drimmel, R., Jansen, F., Katz, D., Lattanzi, M. G., van Leeuwen, F., Bakker, J., Cacciari, C., Castañeda, J., De Angeli, F., Fabricius, C., Fouesneau, M., Frémat,

Y., Galluccio, L., Guerrier, A., Heiter, U., Masana, E., Messineo, R., Mowlavi, N., Nicolas, C., Nienartowicz, K., Pailler, F., Panuzzo, P., Riclet, F., Roux, W., Seabroke, G. M., Sordo, R., Thévenin, F., Gracia-Abril, G., Portell, J., Teyssier, D., Altmann, M., Andrae, R., Audard, M., Bellas-Velidis, I., Benson, K., Berthier, J., Blomme, R., Burgess, P. W., Busonero, D., Busso, G., Cánovas, H., Carry, B., Cellino, A., Cheek, N., Clementini, G., Damerdji, Y., Davidson, M., de Teodoro, P., Nuñez Campos, M., Delchambre, L., Dell'Oro, A., Esquej, P., Fernández-Hernández, J., Fraile, E., Garabato, D., García-Lario, P., Gosset, E., Haigron, R., Halbwachs, J. L., Hambly, N. C., Harrison, D. L., Hernández, J., Hestroffer, D., Hodgkin, S. T., Holl, B., Janßen, K., Jevardat de Fombelle, G., Jordan, S., Krone-Martins, A., Lanzafame, A. C., Löffler, W., Marchal, O., Marrese, P. M., Moitinho, A., Muinonen, K., Osborne, P., Pancino, E., Pauwels, T., Recio-Blanco, A., Reylé, C., Riello, M., Rimoldini, L., Roegiers, T., Rybizki, J., Sarro, L. M., Siopis, C., Smith, M., Sozzetti, A., Utrilla, E., van Leeuwen, M., Abbas, U., Ábrahám, P., Abreu Aramburu, A., Aerts, C., Aguado, J. J., Ajaj, M., Aldea-Montero, F., Altavilla, G., Álvarez, M. A., Alves, J., Anders, F., Anderson, R. I., Anglada Varela, E., Antoja, T., Baines, D., Baker, S. G., Balaguer-Núñez, L., Balbinot, E., Balog, Z., Barache, C., Barbato, D., Barros, M., Barstow, M. A., Bartolomé, S., Bassilana, J. L., Bauchet, N., Becciani, U., Bellazzini, M., Berihuete, A., Bernet, M., Bertone, S., Bianchi, L., Binnenfeld, A., Blanco-Cuaresma, S., Blazere, A., Boch, T., Bombrun, A., Bossini, D., Bouquillon, S., Bragaglia, A., Bramante, L., Breedt, E., Bressan, A., Brouillet, N., Brugaletta, E., Bucciarelli, B., Burlacu, A., Butkevich, A. G., Buzzi, R., Caffau, E., Cancelliere, R., Cantat-Gaudin, T., Carballo, R., Carlucci, T., Carnerero, M. I., Carrasco, J. M., Casamiquela, L., Castellani, M., Castro-Ginard, A., Chaoul, L., Charlot, P., Chemin, L., Chiaramida, V., Chiavassa, A., Chornay, N., Comoretto, G., Contursi, G., Cooper, W. J., Cornez, T., Cowell, S., Crifo, F., Cropper, M., Crosta, M., Crowley, C., Dafonte, C., Dapergolas, A., David, M., David, P., de Laverny, P., De Luise, F., De March, R., De Ridder, J., de Souza, R., de Torres, A., del Peloso, E. F., del Pozo, E., Delbo, M., Delgado, A., Delisle, J. B., Demouchy, C., Dharmawardena, T. E., Di Matteo, P., Diakite, S., Diener, C., Distefano, E., Dolding, C., Edvardsson, B., Enke, H., Fabre, C., Fabrizio, M., Faigler, S., Fedorets, G., Fernique, P., Fienga, A., Figueras, F., Fournier, Y., Fouron, C., Fragkoudi, F., Gai, M., Garcia-Gutierrez, A., Garcia-Reinaldos, M., García-Torres, M., Garofalo, A., Gavel, A., Gavras, P., Gerlach, E., Geyer, R., Giacobbe, P., Gilmore, G., Girona, S., Giuffrida, G., Gomel, R., Gomez, A., González-Núñez, J., González-Santamaría, I., González-Vidal, J. J., Granvik, M., Guillout, P., Guiraud, J., Gutiérrez-Sánchez, R., Guy, L. P., Hatzidimitriou, D., Hauser, M., Haywood, M., Helmer, A., Helmi, A., Sarmiento, M. H., Hidalgo, S. L., Hilger, T., Hładczuk, N., Hobbs, D., Holland, G., Huckle, H. E., Jardine, K., Jasniewicz, G., Jean-Antoine Piccolo, A., Jiménez-Arranz, Ó., Jorissen, A., Juaristi Campillo, J., Julbe, F., Karbevska, L., Kervella, P., Khanna,

S., Kontizas, M., Kordopatis, G., Korn, A. J., Kóspál, Á., Kostrzewa-Rutkowska, Z., Kruszyńska, K., Kun, M., Laizeau, P., Lambert, S., Lanza, A. F., Lasne, Y., Le Campion, J. F., Lebreton, Y., Lebzelter, T., Leccia, S., Leclerc, N., Lecoeur-Taibi, I., Liao, S., Licata, E. L., Lindstrøm, H. E. P., Lister, T. A., Livanou, E., Lobel, A., Lorca, A., Loup, C., Madrero Pardo, P., Magdaleno Romeo, A., Managau, S., Mann, R. G., Manteiga, M., Marchant, J. M., Marconi, M., Marcos, J., Marcos Santos, M. M. S., Marín Pina, D., Marinoni, S., Marocco, F., Marshall, D. J., Martin Polo, L., Martín-Fleitas, J. M., Marton, G., Mary, N., Masip, A., Massari, D., Mastrobuono-Battisti, A., Mazeh, T., McMillan, P. J., Messina, S., Michalik, D., Millar, N. R., Mints, A., Molina, D., Molinaro, R., Molnár, L., Monari, G., Monguió, M., Montegriffo, P., Montero, A., Mor, R., Mora, A., Morbidelli, R., Morel, T., Morris, D., Muraveva, T., Murphy, C. P., Musella, I., Nagy, Z., Noval, L., Ocaña, F., Ogden, A., Ordenovic, C., Osinde, J. O., Pagani, C., Pagano, I., Palaversa, L., Palicio, P. A., Pallas-Quintela, L., Panahi, A., Payne-Wardenaar, S., Peñalosa Esteller, X., Penttilä, A., Pichon, B., Piersimoni, A. M., Pineau, F. X., Plachy, E., Plum, G., Poggio, E., Prša, A., Pulone, L., Racero, E., Ragaini, S., Rainer, M., Raiteri, C. M., Rambaux, N., Ramos, P., Ramos-Lerate, M., Re Fiorentin, P., Regibo, S., Richards, P. J., Rios Diaz, C., Ripepi, V., Riva, A., Rix, H. W., Rixon, G., Robichon, N., Robin, A. C., Robin, C., Roelens, M., Rogues, H. R. O., Rohrbasser, L., Romero-Gómez, M., Rowell, N., Royer, F., Ruz Mieres, D., Rybicki, K. A., Sadowski, G., Sáez Núñez, A., Sagristà Sellés, A., Sahlmann, J., Salguero, E., Samaras, N., Sanchez Gimenez, V., Sanna, N., Santoveña, R., Sarasso, M., Schultheis, M., Sciacca, E., Segol, M., Segovia, J. C., Ségransan, D., Semeux, D., Shahaf, S., Siddiqui, H. I., Siebert, A., Siltala, L., Silvelo, A., Slezak, E., Slezak, I., Smart, R. L., Snaith, O. N., Solano, E., Solitro, F., Souami, D., Souchay, J., Spagna, A., Spina, L., Spoto, F., Steele, I. A., Steidelmüller, H., Stephenson, C. A., Süveges, M., Surdej, J., Szabados, L., Szegedi-Elek, E., Taris, F., Taylor, M. B., Teixeira, R., Tolomei, L., Tonello, N., Torra, F., Torra, J., Torralba Elipe, G., Trabucchi, M., Tsounis, A. T., Turon, C., Ulla, A., Unger, N., Vaillant, M. V., van Dillen, E., van Reeven, W., Vanel, O., Vecchiato, A., Viala, Y., Vicente, D., Voutsinas, S., Weiler, M., Wevers, T., Wyrzykowski, Ł., Yoldas, A., Yvard, P., Zhao, H., Zorec, J., Zucker, S., and Zwitter, T. (2023). Gaia Data Release 3. Summary of the content and survey properties. *aap*, 674:A1.

Ginsburg, A., Sipőcz, B. M., Brasseur, C. E., Cowperthwaite, P. S., Craig, M. W., Deil, C., Guillochon, J., Guzman, G., Liedtke, S., Lian Lim, P., Lockhart, K. E., Mommert, M., Morris, B. M., Norman, H., Parikh, M., Persson, M. V., Robitaille, T. P., Segovia, J.-C., Singer, L. P., Tollerud, E. J., de Val-Borro, M., Valtchanov, I., Woillez, J., The Astroquery collaboration, and a subset of the astropy collaboration (2019). astroquery: An Astronomical Web-querying Package in Python. *The Astronomical Journal*, 157:98.

Halpern, J. P., Perez, K. I., and Bogdanov, S. (2022). Luminous Optical and X-ray Flaring of the Putative Redback Millisecond Pulsar 1FGL J0523.5$-$2529. *The Astrophysical Journal*, 935(2):151. arXiv:2207.08198 [astro-ph].

Heger, A., Fryer, C. L., Woosley, S. E., Langer, N., and Hartmann, D. H. (2003). How Massive Single Stars End Their Life. *The Astrophysical Journal*, 591:288–300. ADS Bibcode: 2003ApJ...591..288H.

Hewish, A., Bell, S. J., Pilkington, J. D. H., Scott, P. F., and Collins, R. A. (1968). Observation of a Rapidly Pulsating Radio Source. *Nature*, 217(5130):709–713.

Johnson, O. A., Gajjar, V., Keane, E. F., McKenna, D. J., Giese, C., McKeon, B., Carozzi, T. D., Alcaria, C., Brennan, A., Brzycki, B., Croft, S., Drew, J., Elkins, R., Gallagher, P. T., Kelly, R., Lebofsky, M., MacMahon, D. H. E., McCauley, J., Pater, I. d., Raeside, S. R., Siemion, A. P. V., and Worden, S. P. (2023). A Simultaneous Dual-site Technosignature Search Using International LOFAR Stations. *The Astronomical Journal*, 166(5):193. Publisher: The American Astronomical Society.

Karpova, A. V., Zyuzin, D. A., Shibanov, Y. A., and Gilfanov, M. R. (2023). A new redback pulsar candidate 4FGL J2054.2+6904. *Monthly Notices of the Royal Astronomical Society*, 524(2):3020–3025. arXiv:2306.17593 [astro-ph].

Kaspi, V. M., Roberts, M. E., Vasisht, G., Gotthelf, E. V., Pivovaroff, M., and Kawai, N. (2001). Chandra X-Ray Observations of G11.2-0.3: Implications for Pulsar Ages. *The Astrophysical Journal*, 560:371–377. ADS Bibcode: 2001ApJ...560..371K.

Kasting, J. F., Whitmire, D. P., and Reynolds, R. T. (1993). Habitable Zones around Main Sequence Stars. *Icarus*, 101(1):108–128.

Kavanagh, R. D. and Vedantham, H. K. (2023). Hunting for exoplanets via magnetic star–planet interactions: geometrical considerations for radio emission. *Monthly Notices of the Royal Astronomical Society*, 524(4):6267–6284.

Lattimer, J. M. and Prakash, M. (2001). Neutron Star Structure and the Equation of State. *The Astrophysical Journal*, 550(1):426.

Lebofsky, M., Croft, S., Siemion, A. P. V., Price, D. C., Enriquez, J. E., Isaacson, H., MacMahon, D. H. E., Anderson, D., Brzycki, B., Cobb, J., Czech, D., DeBoer, D., DeMarines, J., Drew, J., Foster, G., Gajjar, V., Gizani, N., Hellbourg, G., Korpela, E. J., Lacki, B., Sheikh, S., Werthimer, D., Worden, P., Yu, A., and Zhang, Y. G. (2019). The Breakthrough Listen Search for Intelligent Life: Public Data, Formats, Reduction, and Archiving. *PASP*, 131(1006):124505.

Li, J.-K., Zhao, H.-C., Tao, Z.-Z., Zhang, T.-J., and Xiao-Hui, S. (2022). Drift Rates of Narrowband Signals in Long-term SETI Observations for Exoplanets. *The Astrophysical Journal*, 938(1):1.

Lorimer, D. R. and Kramer, M. (2004). *Handbook of Pulsar Astronomy*, volume 4. Cambridge University Press.

McKenna, D. J., Keane, E. F., Gallagher, P. T., and McAuley, J. (2023). udpPacketManager: An International LOFAR Station Data (Pre-)Processor. *The Journal of Open Source Software*.

Michel, F. C. (1982). Theory of pulsar magnetospheres. *Reviews of Modern Physics*, 54(1):1–66. Publisher: American Physical Society.

Murphy, P. C., Carley, E. P., Ryan, A. M., Zucca, P., and Gallagher, P. T. (2021). LOFAR observations of radio burst source sizes and scattering in the solar corona. *Astronomy and Astrophysics*, 645:A11. ADS Bibcode: 2021A&A...645A..11M.

Ng, C., Rizk, L., Mannion, C., and Keane, E. F. (2022). Search for Extraterrestrial Intelligence with the ngVLA. *The Astronomical Journal*, 164:205. ADS Bibcode: 2022AJ....164..205N.

Oppenheimer, J. R. and Volkoff, G. M. (1939). On Massive Neutron Cores. *Physical Review*, 55(4):374–381. Publisher: American Physical Society.

Ransom, S. M. (2001). *New search techniques for binary pulsars*. PhD thesis. Publication Title: Ph.D. Thesis ADS Bibcode: 2001PhDT.....123R.

Ray, P. S., Abdo, A. A., Parent, D., Bhattacharya, D., Bhattacharyya, B., Camilo, F., Cognard, I., Theureau, G., Ferrara, E. C., Harding, A. K., Thompson, D. J., Freire, P. C. C., Guillemot, L., Gupta, Y., Roy, J., Hessels, J. W. T., Johnston, S., Keith, M., Shannon, R., Kerr, M., Michelson, P. F., Romani, R. W., Kramer, M., McLaughlin, M. A., Ransom, S. M., Roberts, M. S. E., Parkinson, P. M. S., Ziegler, M., Smith, D. A., Stappers, B. W., Weltevrede, P., and Wood, K. S. (2012). Radio Searches of Fermi LAT Sources and Blind Search Pulsars: The Fermi Pulsar Search Consortium. arXiv:1205.3089 [astro-ph].

Ricker, G. R., Winn, J. N., Vanderspek, R., Latham, D. W., Bakos, G. Á., Bean, J. L., Berta-Thompson, Z. K., Brown, T. M., Buchhave, L., Butler, N. R., Butler, R. P., Chaplin, W. J., Charbonneau, D., Christensen-Dalsgaard, J., Clampin, M., Deming, D., Doty, J., De Lee, N., Dressing, C., Dunham, E. W., Endl, M., Fressin, F., Ge, J., Henning, T., Holman, M. J., Howard, A. W., Ida, S., Jenkins, J. M., Jernigan, G., Johnson, J. A., Kaltenegger, L., Kawai, N., Kjeldsen, H., Laughlin, G., Levine,

A. M., Lin, D., Lissauer, J. J., MacQueen, P., Marcy, G., McCullough, P. R., Morton, T. D., Narita, N., Paegert, M., Palle, E., Pepe, F., Pepper, J., Quirrenbach, A., Rinehart, S. A., Sasselov, D., Sato, B., Seager, S., Sozzetti, A., Stassun, K. G., Sullivan, P., Szentgyorgyi, A., Torres, G., Udry, S., and Villasenor, J. (2015). Transiting Exoplanet Survey Satellite (TESS). *Journal of Astronomical Telescopes, Instruments, and Systems*, 1:014003.

Romani, R. W., Kandel, D., Filippenko, A. V., Brink, T. G., and Zheng, W. (2022). Psr j0952-0607: The fastest and heaviest known galactic neutron star. *The Astrophysical Journal Letters*, 934(2):L17.

Sheikh, S. Z. (2020). Nine axes of merit for technosignature searches. *International Journal of Astrobiology*, 19(3):237–243.

Sheikh, S. Z., Wright, J. T., Siemion, A., and Enriquez, J. E. (2019). Choosing a maximum drift rate in a seti search: Astrophysical considerations. *The Astrophysical Journal*, 884(1):14.

Siemion, A. P. V., Demorest, P., Korpela, E., Maddalena, R. J., Werthimer, D., Cobb, J., Howard, A. W., Langston, G., Lebofsky, M., Marcy, G. W., and Tarter, J. (2013). A 1.1-1.9 GHz SETI Survey of the Kepler Field. I. A Search for Narrow-band Emission from Select Targets. *The Astrophysical Journal*, 767:94.

Strader, J., Chomiuk, L., Sonbas, E., Sokolovsky, K., Sand, D. J., Moskvitin, A. S., and Cheung, C. C. (2014). 1FGL J0523.5-2529: A New Probable Gamma-ray Pulsar Binary. *The Astrophysical Journal*, 788(2):L27. arXiv:1405.5533 [astro-ph].

Takata, J., Li, K. L., Leung, G. C. K., Kong, A. K. H., Tam, P. H. T., Hui, C. Y., Wu, E. M. H., Xing, Y., Cao, Y., Tang, S., Wang, Z., and Cheng, K. S. (2014). Multi-wavelength emissions from the millisecond pulsar binary psr j1023+0038 during an accretion active state. *The Astrophysical Journal*, 785(2):131. Publisher: The American Astronomical Society.

Tarter, J. C. (1996). Project Phoenix: the Australian deployment. In Kingsley, S. A. and Lemarchand, G. A., editors, *Photonics West '96*, pages 24–34. SPIE.

Taylor, J. H. and Manchester, R. N. (1977). Recent observations of pulsars. *Annual Review of Astronomy and Astrophysics*, 15:19–44. ADS Bibcode: 1977ARA&A..15...19T.

van Haarlem, M. P., Wise, M. W., Gunst, A. W., Heald, G., McKean, J. P., Hessels, J. W. T., de Bruyn, A. G., Nijboer, R., Swinbank, J., Fallows, R., Brentjens, M., Nelles, A., Beck, R., Falcke, H., Fender, R., Hörandel, J., Koopmans, L. V. E., Mann, G., Miley, G., Röttgering, H., Stappers, B. W., Wijers, R. a. M. J., Zaroubi, S., van den

Akker, M., Alexov, A., Anderson, J., Anderson, K., van Ardenne, A., Arts, M., Asgekar, A., Avruch, I. M., Batejat, F., Bähren, L., Bell, M. E., Bell, M. R., van Bemmel, I., Bennema, P., Bentum, M. J., Bernardi, G., Best, P., Bîrzan, L., Bonafede, A., Boonstra, A.-J., Braun, R., Bregman, J., Breitling, F., van de Brink, R. H., Broderick, J., Broekema, P. C., Brouw, W. N., Brüggen, M., Butcher, H. R., van Cappellen, W., Ciardi, B., Coenen, T., Conway, J., Coolen, A., Corstanje, A., Damstra, S., Davies, O., Deller, A. T., Dettmar, R.-J., van Diepen, G., Dijkstra, K., Donker, P., Doorduin, A., Dromer, J., Drost, M., van Duin, A., Eislöffel, J., van Enst, J., Ferrari, C., Frieswijk, W., Gankema, H., Garrett, M. A., de Gasperin, F., Gerbers, M., de Geus, E., Grießmeier, J.-M., Grit, T., Gruppen, P., Hamaker, J. P., Hassall, T., Hoeft, M., Holties, H. A., Horneffer, A., van der Horst, A., van Houwelingen, A., Huijgen, A., Iacobelli, M., Intema, H., Jackson, N., Jelic, V., de Jong, A., Juette, E., Kant, D., Karastergiou, A., Koers, A., Kollen, H., Kondratiev, V. I., Kooistra, E., Koopman, Y., Koster, A., Kuniyoshi, M., Kramer, M., Kuper, G., Lambropoulos, P., Law, C., van Leeuwen, J., Lemaitre, J., Loose, M., Maat, P., Macario, G., Markoff, S., Masters, J., McFadden, R. A., McKay-Bukowski, D., Meijering, H., Meulman, H., Mevius, M., Middelberg, E., Millenaar, R., Miller-Jones, J. C. A., Mohan, R. N., Mol, J. D., Morawietz, J., Morganti, R., Mulcahy, D. D., Mulder, E., Munk, H., Nieuwenhuis, L., van Nieuwpoort, R., Noordam, J. E., Norden, M., Noutsos, A., Offringa, A. R., Olofsson, H., Omar, A., Orrú, E., Overeem, R., Paas, H., Pandey-Pommier, M., Pandey, V. N., Pizzo, R., Polatidis, A., Rafferty, D., Rawlings, S., Reich, W., de Reijer, J.-P., Reitsma, J., Renting, G. A., Riemers, P., Rol, E., Romein, J. W., Roosjen, J., Ruiter, M., Scaife, A., van der Schaaf, K., Scheers, B., Schellart, P., Schoenmakers, A., Schoonderbeek, G., Serylak, M., Shulevski, A., Sluman, J., Smirnov, O., Sobey, C., Spreeuw, H., Steinmetz, M., Sterks, C. G. M., Stiepel, H.-J., Stuurwold, K., Tagger, M., Tang, Y., Tasse, C., Thomas, I., Thoudam, S., Toribio, M. C., van der Tol, B., Usov, O., van Veelen, M., van der Veen, A.-J., ter Veen, S., Verbiest, J. P. W., Vermeulen, R., Vermaas, N., Vocks, C., Vogt, C., de Vos, M., van der Wal, E., van Weeren, R., Weggemans, H., Weltevrede, P., White, S., Wijnholds, S. J., Wilhelmsson, T., Wucknitz, O., Yatawatta, S., Zarka, P., Zensus, A., and van Zwieten, J. (2013). LOFAR: The LOw-Frequency ARray. *Astronomy & Astrophysics, Volume 556, id.A2, <NUMPAGES>53</NUMPAGES> pp.*, 556:A2.

Vedantham, H. K., Callingham, J. R., Shimwell, T. W., Tasse, C., Pope, B. J. S., Bedell, M., Snellen, I., Best, P., Hardcastle, M. J., Haverkorn, M., Mechev, A., O'Sullivan, S. P., Röttgering, H. J. A., and White, G. J. (2020). Coherent radio emission from a quiescent red dwarf indicative of star-planet interaction. *Nature Astronomy*, 4:577–583. ADS Bibcode: 2020NatAs...4..577V.

Villadsen, J. and Hallinan, G. (2019). Ultra-wideband Detection of 22 Coherent Radio

Bursts on M Dwarfs. *The Astrophysical Journal*, 871(2):214. Publisher: The American Astronomical Society.

Wlodarczyk-Sroka, B. S., Garrett, M. A., and Siemion, A. P. V. (2020). Extending the Breakthrough Listen nearby star survey to other stellar objects in the field. *MNRAS*, 498(4):5720–5729.

Zarka, P. (1998). Auroral radio emissions at the outer planets: Observations and theories. *Journal of Geophysical Research: Planets*, 103(E9):20159–20194. _eprint: https://onlinelibrary.wiley.com/doi/pdf/10.1029/98JE01323.

Zhelezniakov, V. V. and Zlotnik, E. I. (1975). Cyclotron Wave Instability in the Corona and Origin of Solar Radio Emission with Fine Structure. I: Bernstein Modes and Plasma Waves in a Hybrid Band. 43(2):431–451.